Research Article

Jiawei Chen, Jinming Xu*, and Jizhong Huang

Microscopic mechanism of sandstone hydration in Yungang Grottoes, China

https://doi.org/10.1515/geo-2020-0158
received October 24, 2019; accepted May 24, 2020

Abstract: The macroscopic engineering properties of sandstone are dominated primarily by mineral features in a microscopic scale. This study will investigate the microscopic physical and mechanical properties of the main minerals (quartz, K-feldspar, Na-feldspar and kaolinite) in Yungang Grottoes sandstone, using the molecular mechanics and the molecular dynamics simulations. The microscopic physical properties were represented by density and volume. The microscopic mechanical properties were represented by Young's modulus and Poisson's ratio. The microscopic mechanical properties of the minerals in various directions were then explored. The influences of water molecules and the surrounding temperature on the microscopic physical and mechanical properties of the minerals were furthermore investigated. It is found that the differences in the microscopic densities between the simulated results and those from the open data set are, respectively, 0.37%, 1.15% and 9.16%, for the quartz, Na-feldspar and kaolinite cells; the microscopic mechanical properties of various minerals have a significant anisotropy; the Young's modulus of halloysite decreases by 75.86% compared with that of kaolinite; as the water molecule number increased from 0 to 5, the Young's moduli of K-feldspar, Na-feldspar and kaolinite cells decreases by 31.31%, 55.05% and 42.60%, respectively; for each mineral, as the temperature increases from 243.15 to 303.15 K under one atmospheric pressure, the volume increases and the density decreases. Those results may have a theoretical significance for the analysis of microscopic mechanism of hydration in the Yungang Grottoes sandstone.

Keywords: sandstone, hydration, molecular simulation, Yungang

*** Corresponding author: Jinming Xu,** Department of Civil Engineering, Shanghai University, Shanghai, 200444, China, e-mail: xjming@163.com, tel: +86 18516677858
Jiawei Chen: Department of Civil Engineering, Shanghai University, Shanghai, 200444, China
Jizhong Huang: Institute for the Conservation of Cultural Heritage, Shanghai University, Shanghai, 200444, China

1 Introduction

Yungang Grottoes reflects both the artistic style of the early grottoes in China from the middle fifth to early sixth centuries and the blooming religious culture in the northern China. This grotto is one of the most important cultural heritages in China, which has great artistic, scientific and cultural values. Naturally weathering is a severe problem during the preservation of rock relics of the Yungang Grottoes.

Yungang Grottoes is located in Datong City, Shanxi Province, China. It possesses a continental semi-arid monsoon climate. The rainy months are from July to September, with an average annual precipitation and evaporation of 423 and 1,746 mm, respectively [1]. The water types in the Yungang Grottoes sandstone are mainly stagnant water in the weathered rock mass, condensate water, capillary water and so on. Various types of water interact with minerals in the sandstone. The hydration becomes a main cause of the weathering in Yungang Grottoes [2].

The hydration of sandstone has been investigated from various aspects. Rao [3] used the environmental scanning electron microscopy to observe the weathering process of sandstone; Grafchikov et al. [4] investigated the weathering process of sandstone by X-ray fluorescence and other techniques; McCabe et al. [5] investigated the influence of climate on the sandstone weathering in the UK; Barone et al. [6] explored the effect of salt crystallization on the physical and mechanical properties of sandstone during weathering and Sato and Hattanji [7] investigated the weathering processes caused by different minerals.

Most of the existing works related to the hydration in Yungang Grottoes are focused on the macroscopic scale. For example, Wang et al. [8] explored the effects of temperature and moisture on the relics; Guo and Jiang [1] investigated the effects of the water content and salinity on sandstone weathering; Yang et al. [9] examined the effect of water on the long-term strength of the rock column and Yang et al. [10] demonstrated the reflectance spectroscopy during the monitoring of a sandstone weathering process.

However, the macroscopic properties of the Yungang Grottoes sandstone depend primarily on the physical and

mechanical properties of minerals in a microscopic scale [11]. Those in the microscopic scale should be paid more attentions. In this study, the types and contents of the minerals will be determined using X-ray diffraction (XRD). The molecular mechanic (MM) and molecular dynamic (MD) simulations will be carried out using the software Material Studio. The unit cells and super cells of the minerals will be then established and optimized. Using MM simulations, the microscopic physical and mechanical properties of minerals will be obtained, and the microscopic mechanical properties of minerals in various directions will also be explored. The influences of water molecules and temperature on the microscopic physical and mechanical properties are furthermore examined, respectively, by the use of MM and MD simulations. The hydration mechanism of the sandstones is thereafter investigated in a microscopic scale.

2 Methodology

2.1 Materials

The physical and mechanical properties of the Yungang Grottoes sandstone are much related to the mineral contents and weathering magnitudes.

To obtain the mineral types and contents of the Yungang Grottoes sandstones, the samples at Grottoes 1, 2, 3, 5, 7, 12, 14, 17, 19, 21, 23, 29 and 39 were collected. The XRD tests for these sandstones were conducted by the PetroChina Research Institute of Petroleum Exploration and Development.

To determine the weathering magnitudes of those samples, according to the P-wave velocity ratio of weathered rock to fresh rock, the weathering magnitude of the sandstone in Yungang Grottoes can be classified as 1–9 grades or Grade 1 (fresh), Grade 2 (slightly weathered), Grade 3–4 (moderately weathered), Grade 5–6 (highly weathered), Grade 7–8 (completely weathered) and Grade 9 (residual soil) [12]. As the velocity ratio falls, the weathering grade increases and weathering magnitude decreases.

2.2 Microscopic physical and mechanical properties of minerals

2.2.1 Establishment and optimization of models

The physical and mechanical properties of minerals in the sandstone in the macroscopic scale are mainly determined by those in the microscopic scale. To investigate the microscopic physical and mechanical properties of minerals, the unit cell and super cell models should be established according to the Crystallography Open Database [13]. The size of a super cell may affect the simulation result [14]. To reduce errors, for each mineral, the super cell is constructed by 64 unit cells in a style of $4A \times 4B \times 4C$.

In nature, molecules usually exist with low energy in a stable state. Therefore, the unit cells and super cells need to take geometric optimization so as to minimize the energy. To minimize the energy, it is necessary to compute the atomic interactions between the unit cells and super cells. The interaction forces exerted by other atoms are associated with the positions. The universal force field (UFF) [15] was used in the study to describe the potential energy, demonstrating in the function of atom coordinates. The potential energy of UFF is given by equation (1):

$$E = E_{\mathrm{b}} + E_{\mathrm{a}} + E_{\mathrm{t}} + E_{\mathrm{i}} + E_{\mathrm{e}} + E_{\mathrm{v}} \tag{1}$$

where E is the potential energy, E_{b} is the bond's stretching energy, E_{a} is the bending potential energy of bond angles, E_{t} is the distortion potential energy of normal dihedral angle, E_{i} is the distortion potential energy of abnormal dihedral angle, E_{e} is the potential energy of Coulomb action and E_{v} is the potential energy of van der Waals action. Bonding interaction may be described by the first four terms, while non-bonding interaction may be described by the last two terms.

The Coulomb energy between the two point charges may be obtained by equation (2):

$$E_{\mathrm{e}} = k_{\mathrm{e}} q_1 q_2 / (R^2) \tag{2}$$

where k_{e} is the Coulomb constant, q_1 and q_2 are the volumes of two point charges and R is the distance between two point charges.

The potential energy of the van der Waals may be obtained by the Lennard–Jones potential (12-6) [16] (see equation (3)):

$$U(r) = 4\varepsilon\left[\left(\frac{\sigma}{r}\right)^{12} - \left(\frac{\sigma}{r}\right)^{6}\right] \tag{3}$$

where r is the distance between atoms, ε is the minimum value of potential function and σ is the value of r when the potential function equals to 0.

To optimize unit cell, the MM simulation configurations were set up as follows in the software Material Studio. The smart method was adopted to improve the precision. Electrostatic forces between the point charges were computed by Ewald Sum method [17], with the

precision of 10^{-5} kcal/mol. van der Waals energy was obtained based on the atom method. To speedup the computation of van der Waals energy, it is necessary to set the cutoff distance. The reason is that both the attractive forces and the repulsive forces weaken rapidly with an increase in distance r (see equation (3)), although an atom interacts with all atoms in the molecule. Then the forces of the two molecules are computed only within the cutoff distance. According to the nearest image convention, the cutoff distance should be less than the half of the shortest cell length. Therefore, the unit cell cutoff distances of quartz, K-feldspar, Na-feldspar and kaolinite were, respectively, 2.45, 3.55, 3.55 and 2.55 Å. Super cell cutoff distances of those minerals were all 12.5 Å, with spline width = 1 Å and buffer width = 0.5 Å. The external pressure was set at 0 GPa. The number of iteration steps was set at 300. After optimization, the stable conformations of unit cells and super cells were then obtained for the later computations.

2.2.2 Computations of physical properties of minerals

Microscopic physical properties of minerals were represented by volumes and densities in the study. Known the cell lengths, the angles between edges and masses (M) of the optimized unit cells and super cells, the volume (V) and the densities (ρ) are obtained, respectively, by equations (4) and (5):

$$V = abc \cdot \sin\alpha \sin\beta \sin\gamma \tag{4}$$

$$\rho = M/V \tag{5}$$

where a, b and c are the axes lengths of cells, respectively; α, β and γ are the included angles of the axes, respectively.

2.2.3 Computations of mechanical properties of minerals

Microscopic mechanical properties of minerals were represented by Young's modulus and Poisson's ratio in the study. Computations were based on Theodorou and Suter's method [18], which assumes the stress–strain relation satisfies the generalized Hooke's law. Set the time of strain at nine and the maximum strain amplitude at 0.4%. The elastic properties related to stress and strain may be obtained by equations (6) and (7):

$$C_{lmnk} = \frac{\partial\sigma_{lm}}{\partial\sigma_{nk}}\bigg|_{T,\varepsilon_{nk}} = \frac{1}{V_0}\frac{\partial^2 A}{\partial\varepsilon_{lm}\partial\varepsilon_{nk}}\bigg|_{T,\varepsilon_{lm},\varepsilon_{nk}} \tag{6}$$

$$S_{lmnk} = C^{-1}_{lmnk} \tag{7}$$

where T = initial temperature, V_0 = the volume of initial mineral cell, A = Helmholtz free energy, defined as the deformation potential energy, σ_{lm} and σ_{nk} (l, m, n, k = 1, 2, 3, 4, 5, 6) = the stresses applied on cells and ε_{lm} and ε_{lm} = the corresponding strains, –1 = the inverse matrix.

Thus, the stiffness matrix C_{lmnk} and the flexibility matrix S_{lmnk} were obtained. The minerals are usually polycrystalline, the Voigt–Reuss–Hill (VRH) [19,20] approximation method was then used to compute the elastic constants, namely, the bulk moduli K and the shear modui G. The VRH approximation method may be described as equations (8) and (9):

$$K = (K_V + K_R)/2 \tag{8}$$

$$G = (G_V + G_R)/2 \tag{9}$$

where V and R are the moduli of cells in Voigt and Reuss obtained by equations (10)–(13). The second-order tensors C_{ij} and S_{ij} in equations (10)–(13) are, respectively, reduced from the fourth-order tensors C_{lmnk} and S_{lmnk} in equations (6) and (7), considering the symmetry of the stress and strains.

$$9K_V = (C_{11} + C_{22} + C_{33}) + 2(C_{12} + C_{23} + C_{31}) \tag{10}$$

$$15G_V = (C_{11} + C_{22} + C_{33}) - (C_{12} + C_{23} + C_{31}) + 3(C_{44} + C_{55} + C_{66}) \tag{11}$$

$$1/K_R = (S_{11} + S_{22} + S_{33}) + 2(S_{12} + S_{23} + S_{31}) \tag{12}$$

$$15/G_R = 4(S_{11} + S_{22} + S_{33}) - 2(S_{12} + S_{23} + S_{31}) + 3(S_{44} + S_{55} + S_{66}) \tag{13}$$

The Young's modulus E and Poisson's ratio υ were obtained by equations (14) and (15) [21]:

$$E = 9KG/(3K + G) \tag{14}$$

$$\upsilon = (3K - E)/(6K) \tag{15}$$

2.2.4 Water and temperature influences

Considering the interlayer water and adsorbed water may influence the mechanical properties of minerals, the sorption module in the Material Studio was then used for simulations. The water molecules were geometrically optimized before simulations. Because the water and mineral molecules were small, the Metropolis method was adopted. The interlayer water molecules were inserted into the minerals. For the adsorbed water, considering that the hydration radius is 3.0 to 4.5 Å, new unit cells were established with $b_w = b + 4.5$ Å, which is the length of unit cell with adsorbed water molecules. Other original unit cell parameters remain unchanged.

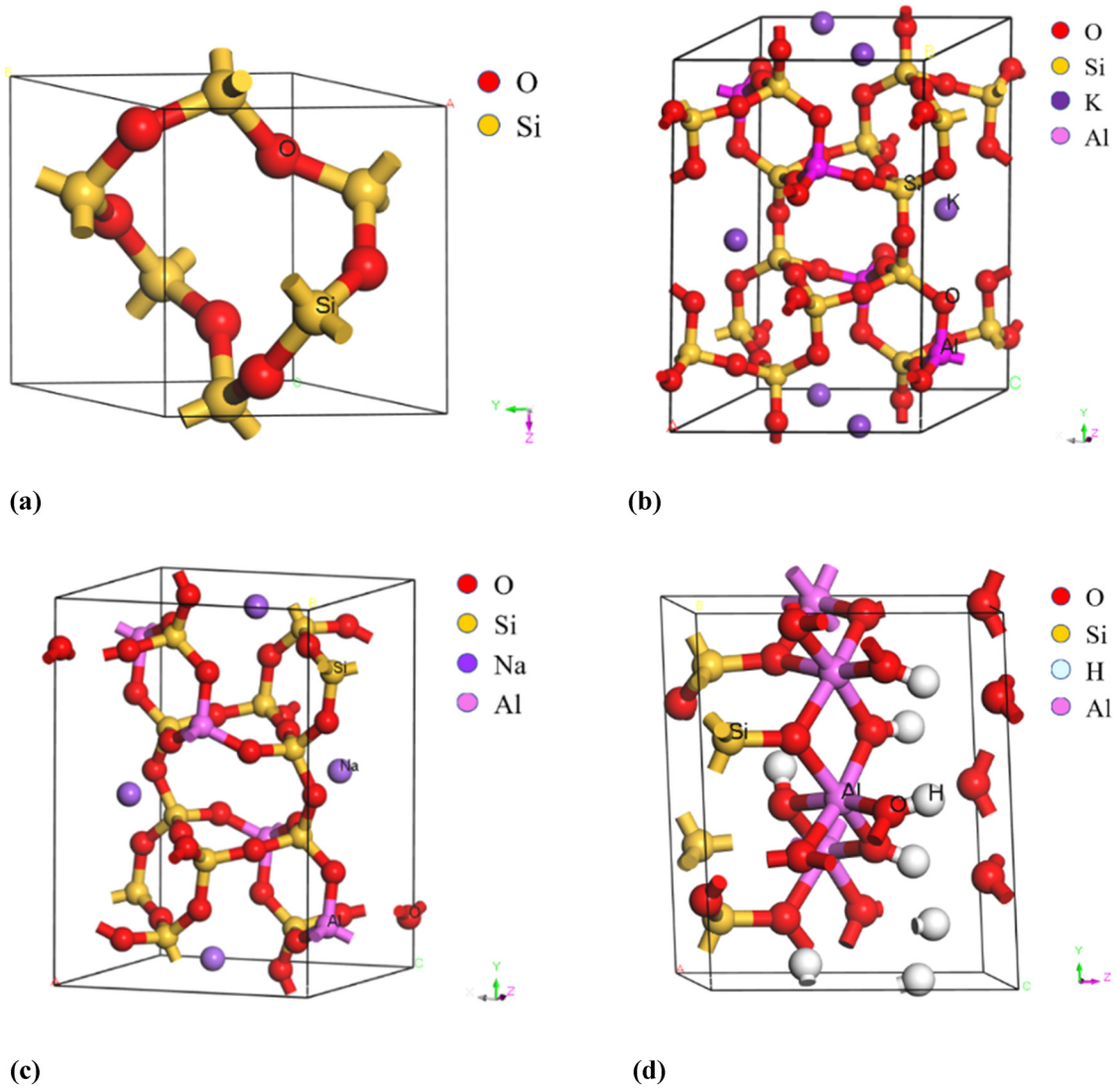

Figure 1: Unit cells of minerals (a) unit cell of quartz (b) unit cell of K-felspar (c) unit cell of Na-feldspar (d) unit-cell of kaolinite.

In the simulations, the mineral unit cells may adsorb up to five water molecules. Unit cells of minerals with 1, 3 and 5 adsorbed water molecules were thereafter established.

In the study, the MD simulation was used to investigate the influence of temperature on the microscopic physical and mechanical properties of minerals, the *NPT* (number of particles *N*, pressure *P* and temperature *T*) ensemble was used to simulate the microscopic physical and mechanical properties of minerals, and the Nose–Hoover and Berendsen methods [22,23] were adopted to control the temperature and pressure, respectively. The time step and total time were set at 1.0 fs and 200 ps, respectively. The initial velocity of system was then obtained by the Maxwell–Boltzmann distribution randomly. Because the weathering occurs on the surface layer of Yungang Grottoes sandstone as the temperature varies from −30°C to 30°C, the simulations were carried out at 243.15, 273.15 and 303.15 K under one atmospheric pressure.

3 Results and discussion

3.1 Formation and optimization

According to the test results of XRD, it is found that quartz, feldspar (K-feldspar and Na-feldspar) and kaolinite are the main minerals of Yungang Grottoes sandstone. The unit cells and super cells of those minerals were established.

For unit cells, the chemical formula of quartz is SiO_2, belonging to the triclinic system with the space group of *P*3121. The lattice parameters of the quartz unit cell are that $\alpha = \beta = 90°$, $\gamma = 120°$, $a = b = 4.913$ Å and $c = 5.404$ Å. The quartz unit cell is shown in Figure 1(a).

The chemical formula of K-feldspar is $KAlSi_3O_8$, belonging to the monoclinic system with the space group of *C*2/*m*. The lattice parameters of K-feldspar unit cell are that $\alpha = 90°$, $\beta = 116.1°$, $\gamma = 90°$, $a = 8.45$ Å, $b = 12.9$ Å and $c = 7.15$ Å. Normally, feldspar is in disorder at high temperature while in order at low temperature. In this study, the K-feldspar and Na-feldspar models have rather high-order degrees. The K-feldspar unit cell is shown in Figure 1(b).

The chemical formula of Na-feldspar is $NaAlSi_3O_8$, belonging to the triclinic system with the space group of C1. The lattice parameters of Na-feldspar unit cell are that $\alpha = 94.245°$, $\beta = 116.605°$, $\gamma = 87.809°$, $a = 8.137$ Å, $b = 12.787$ Å and $c = 7.157$ Å. The unit cell of Na-feldspar is shown in Figure 1(c).

The chemical formula of kaolinite is $Al_4[Si_4O_{10}](OH)_8$, belonging to the triclinic system with the space group of P1. The lattice parameters of kaolinite unit cell are that $\alpha = 91.684°$, $\beta = 105.128°$, $\gamma = 89.7549°$, $a = 5.174$ Å, $b = 8.985$ Å and $c = 7.352$ Å. The unit cell of kaolinite is shown in Figure 1(d).

All super cells of minerals were then configured. The quartz super cell is taken as an example to be shown in Figure 2.

The potential energies of quartz unit cell and super cell before and after the optimization are taken as an example to be shown in Table 1. From Table 1, it can be seen that the potential energies of unit cell are −20.19 kcal mol^{-1} and −28.12 kcal mol^{-1}, respectively, before and after optimization. The potential energies of super cell are −1286.76 kcal mol^{-1} and −1794.14 kcal mol^{-1}, respectively, before and after optimization. The potential energies of unit cell and super cell decreased, respectively, by 39.28% and 39.43% after optimization. The potential energies of both unit cell and super cell decreased greatly in the generation of the stable conformations.

3.2 Microscopic physical and mechanical properties of minerals

3.2.1 Microscopic physical properties of minerals

The microscopic physical properties of the unit and super cells of minerals are listed in Table 2. From Table 2 it can be seen that the volumes of quartz, K-feldspar, Na-feldspar and kaolinite unit-cell are 110.53, 683.21, 672.98 and 299.41 $Å^3$, respectively; the volumes of quartz, K-feldspar, Na-feldspar and kaolinite super cell are 7072.00, 43024.36, 43694.59 and 19146.75 $Å^3$, respectively; the densities of unit cells and super cells of quartz, K-feldspar, Na-feldspar and kaolinite are 2.71, 2.71, 2.59 and 2.86 g cm^{-3}, respectively.

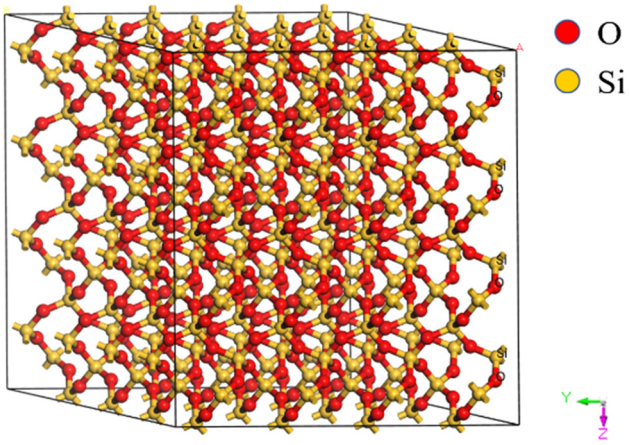

Figure 2: Super cell of quartz.

3.2.2 Verification of microscopic physical properties of minerals

The microscopic densities of quartz, K-feldspar, Na-feldspar and kaolinite cells and super cells obtained by MM simulation were compared with those from the published data set in the macroscopic and microscopic scales (see Table 3).

From Table 3 it can be seen that the densities of quartz, K-feldspar, Na-feldspar and kaolinite in MM simulation are 2.71, 2.71, 2.59 and 2.86 g cm^{-3}, respectively. According to the published data set, the macroscopic density of those are, respectively, 2.65, 2.57, 2.61 and 2.68 g cm^{-3} or lower 2.26%, lower 5.45%, higher 0.77% and lower 6.71% than those, respectively, from the MM simulations; the densities of quartz, Na-feldspar and kaolinite are, respectively, 2.70 g cm^{-3} [24], 2.62 g cm^{-3} [25] and 2.62 g cm^{-3} [26], or lower 0.37%, greater 1.15% and lower 9.16% than those, respectively, from the MM simulation.

In summary, the microscopic densities of unit and super cells of quartz, K-feldspar, Na-feldspar and kaolinite obtained by the MM simulation agree well with the published data set. The differences between the simulated results and the published data set may be caused by the following factors. (1) In a natural state, it

Table 1: Potential energies of unit cell and super cell of quartz before and after optimization

Energy type	Potential energy of unit cell/kcal mol^{-1}		Potential energy of super cell/kcal mol^{-1}	
	Before optimization	After optimization	Before optimization	After optimization
Bond	4.07	0.08	260.51	5.57
Angle	2.53	0.03	161.89	2.05
Torsion	1.25	1.20	80.24	76.72
Inversion	0.00	0.00	0.00	0.00
Electrostatic	0.00	0.00	0.00	0.00
van der Waals	−28.05	−29.44	−1733.92	−1821.75
Total energy	−20.19	−28.12	−1286.76	−1794.14

Table 2: Microscopic physical properties of unit cells and super cells of various minerals

Mineral type	Cell type	Volume/Å^3	Density/g cm^{-3}
Quartz	Unit cell	110.53	2.71
	Super cell	7072.00	2.71
K-feldspar	Unit cell	683.21	2.71
	Super cell	43024.36	2.71
Na-feldspar	Unit cell	672.98	2.59
	Super cell	43694.59	2.59
Kaolinite	Unit cell	299.41	2.86
	Super cell	19146.75	2.86

is difficult to obtain the density of the pure minerals, and the densities of other minerals may affect the result. (2) The parameters (such as cell lengths and angles) used in the microscopic models of the minerals in the simulation may be different from those in the published data set.

3.2.3 Microscopic mechanical properties of minerals

The microscopic mechanical properties of the unit cells and super cells of minerals were obtained by MM simulation and are shown in Table 4. From Table 4 it can be seen that the Young's moduli of the unit cells of quartz, K-feldspar, Na-feldspar and kaolinite are 215.6, 126.54, 102.56 and 162.12 GPa, respectively; the Young's moduli of the super cells of quartz, K-feldspar, Na-feldspar and kaolinite are 214.16, 126.48, 102.87 and 162.88 GPa, respectively; the Poisson's ratio of unit cells and super cells of quartz, K-feldspar, Na-feldspar and kaolinite are 0.17, 0.23, 0.21 and 0.26, respectively.

3.2.4 Anisotropy

The anisotropy are important mechanical properties of K-feldspar, Na-feldspar and kaolinite because the unit cells of these minerals are, respectively, monoclinic, triclinic and triclinic systems which are highly asymmetric. To investigate anisotropy, the Young's moduli and Poisson's ratios of mineral unit cells were obtained by simulations and are shown in Table 5.

From Table 5 it can be seen that the Young's moduli of K-feldspar in the *Y* and *Z* directions are 3.161 and 5.455 times, respectively, greater than those in the *X* direction; the Young's moduli of the Na-feldspar in the *Y* and *Z*

Table 3: Comparison of physical properties between MM simulation and published data set

Mineral type	Cell type	Density/g cm^{-3}		
		MM simulation	Macroscopic (published data set)	Microscopic (published data set)
Quartz	Unit cell	2.71	2.65	2.70
	Super cell	2.71		
K-felspar	Unit cell	2.71	2.57	—
	Super cell	2.71		
Na-feldspar	Unit cell	2.59	2.61	2.62
	Super cell	2.59		
Kaolinite	Unit cell	2.86	2.68	2.62
	Super cell	2.86		

Table 4: Microscopic mechanical properties of unit cells and super cells of various minerals

Mineral type	Cell type	Young's modulus/GPa	Poisson's ratio
Quartz	Unit cell	215.60	0.17
	Super cell	214.16	0.17
K-feldspar	Unit cell	126.54	0.23
	Super cell	126.48	0.23
Na-feldspar	Unit cell	102.56	0.21
	Super cell	102.87	0.21
Kaolinite	Unit cell	162.12	0.26
	Super cell	162.88	0.26

directions are 5.566 and 8.832 times, respectively, greater than those in the *X* direction; the Young's moduli of kaolinite in the *X* and *Y* directions are 1.972 and 6.442 times, respectively, greater than those in the *Z* direction. Minerals have positive Poisson's ratios in all directions, indicating that their volumes do not expand under external load.

The Poisson's ratios of K-feldspar and Na-feldspar in the *yx* direction are 0.90 and 1.28, respectively, which are obviously greater than the macroscopic Poisson's ratio with the maximum of 0.5. That is partly because the optimized unit cell models used in the calculation have structural defects in some particular directions.

3.2.5 Water and temperature influences

Kaolinite is an octahedron 1:1 layered silicate with a unit structural layer. Halloysite structure is a layer of water molecules sandwiched by two layers of kaolinite. The chemical formula of halloysite is $Al_4[Si_4O_{10}](OH)_8{\cdot}4H_2O$, which has a unit structural layer height of 10.1 Å and a water molecular layer thickness of 2.9 Å. The lattice parameters of halloysite unit cell are $\alpha = 90°$, $\beta = 100°$, $\gamma = 90°$, $a = 5.20$ Å, $b = 8.92$ Å and $c = 10.25$ Å. Considering the influence of the interlayer water on the mechanical properties of kaolinite, a unit cell of halloysite was established and optimized.

Table 5: Unit cell anisotropy of K-feldspar, Na-feldspar and kaolinite

Elastic constants		K-feldspar	Na-feldspar	Kaolinite
Young's modulus/ GPa	Direction *X*	46.16	26.38	134.49
	Direction *Y*	145.89	146.81	439.34
	Direction *Z*	251.81	232.95	68.20
Poisson's ratio	Direction *xy*	0.28	0.23	0.04
	Direction *xz*	0.06	0.03	0.72
	Direction *yx*	0.90	1.28	0.12
	Direction *yz*	0.06	0.09	0.18
	Direction *zx*	0.31	0.27	0.36
	Direction *zy*	0.11	0.14	0.03

The mechanical properties of K-feldspar, Na-feldspar, kaolinite and halloysite's unit cells with various absorbed water molecules were obtained (see Table 6). From Table 6 it can be seen that, as adsorbed water molecules increases from 0 to 5, the Young's moduli of K-feldspar, Na-feldspar, kaolinite and halloysite decrease by 73.77%, 72.80%, 42.60% and 47.46%, respectively; the Poisson's ratios of K-feldspar and halloysite are almost unchanged; the Poisson's ratio of Na-feldspar increase by 14.25% and that of kaolinite decrease by 11.54%.

Microscopic physical and mechanical properties of the unit cells of minerals at various temperatures were also obtained (see Table 7). From Table 7 it can be seen that as temperature rises from 243.15 to 303.15 K, the volume of the unit cell of quartz, K-feldspar, Na-feldspar and kaolinite increases by 0.25%, 0.23%, 0.17% and 0.31%, respectively; the density of these minerals decreases by 0.26%, 0.22%, 0.15% and 0.28%, respectively; the Young's moduli of these minerals decrease by 0.12%, unchange, increase by 0.17% and decrease by 7.53%, respectively; the Poisson's ratio of these minerals decreases by 1.18%, unchanges, decreases by 0.48% and increases by 3.85%, respectively.

3.3 Relation between weathering magnitudes and mineral contents of Yungang Grottoes sandstone

Weathering magnitudes of sandstones at various grotto locations were classified (see Figure 3). From Figure 3 it can be seen that the weathering magnitudes of Yungang Grottoes sandstone mainly concentrate on Grades 3–6, namely moderately weathered (Grades 3–4) and highly weathered (Grades 5–6). The number of weathering grottoes with Grade 5 is the largest, with a total of six. It is found that the weathering magnitudes of the grottoes are generally high.

Grades 3 and 6, respectively, at grottoes 14 and 29 were selected to investigate the relation between the weathering grades and mineral contents of those sandstones in Yungang Grottoes because the weathering magnitudes in these two grottoes are quite different. The photographs of these two grottoes are shown in Figure 4. The corresponding weathering grades and mineral contents are listed in Table 8.

Table 6: Microscopic mechanic properties of mineral unit cells with various absorbed water numbers

Adsorption water numbers	K-feldspar		Na-feldspar		Kaolinite		Halloysite	
	Young's modulus/GPa	Poisson's ratio	Young's modulus/GPa	Poisson's ratio	Young's modulus/GPa	Poisson's ratio	Young's modulus/GPa	Poisson's ratio
0	126.54	0.23	102.56	0.21	162.12	0.26	39.32	0.21
1	47.92	0.27	42.57	0.26	142.81	0.24	29.70	0.24
3	37.50	0.25	36.92	0.28	102.89	0.24	26.24	0.22
5	33.19	0.26	27.90	0.28	93.05	0.23	23.78	0.21

Table 7: Microscopic physical and mechanical properties of minerals at various temperatures

Mineral type	Temperature/K	Volume/Å^3	Density/g cm^{-3}	Young's modulus/GPa	Poisson's ratio
Quartz	243.15	7074.881	2.708	213.419	0.169
	273.15	7088.391	2.702	213.284	0.168
	303.15	7092.814	2.701	213.166	0.167
K-feldspar	243.15	43694.421	2.708	126.613	0.226
	273.15	43768.792	2.703	126.586	0.227
	303.15	43795.886	2.702	126.608	0.226
Na-feldspar	243.15	43155.289	2.583	102.771	0.207
	273.15	43164.153	2.582	102.793	0.207
	303.15	43229.563	2.579	102.942	0.206
Kaolinite	243.15	19148.894	2.865	162.637	0.260
	273.15	19193.166	2.859	162.772	0.260
	303.15	19208.333	2.857	150.386	0.270

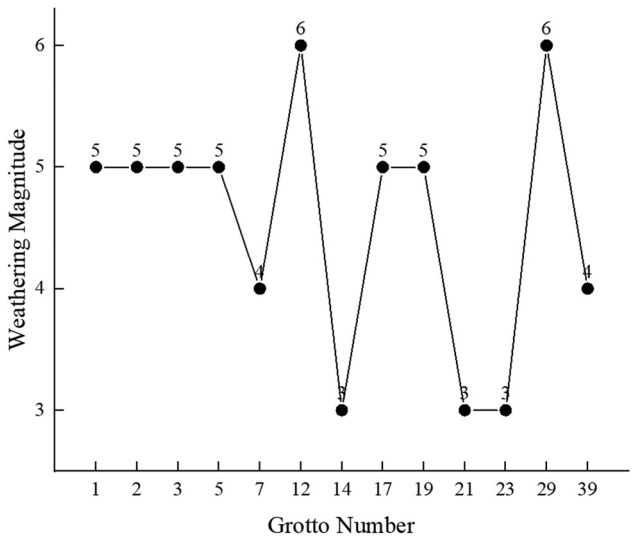

Figure 3: Weathering magnitudes of sandstones at various grotto locations.

From Table 8 it can be seen that compared with the weathering Grade 3 with Grade 6, the wave velocity ratio of the weathering Grade 6 decreases by 33.33%, and the contents of quartz, feldspar and kaolinite, respectively, decrease by 13.84%, decrease by 61.11% and increase by 98.54%, and the contents of calcite and ankerite both decrease to 0.

For the weathering Grade 3, the descending order in the mineral contents is listed as quartz, feldspar, kaolinite, ankerite and calcite. In the same way for the weathering Grade 6, the list is quartz, kaolinite, feldspar, ankerite and calcite. For both Grades 3 and 6, the contents of quartz and ankerite are, respectively, the highest and lowest in all minerals.

3.4 Microscopic mechanism of sandstone hydration in Yungang Grottoes

3.4.1 Microscopic mechanism of macroscopic physical and mechanical properties of minerals

The microscopic physical and mechanical properties of minerals have great implications for the minerals in the macroscopic scale. In this scale, the Young's modulus and Poisson's ratio of the quartz–feldspar sandstone in the horizontal direction is significantly greater than those in the vertical direction [27]. From Table 5 it can be seen that the Young's moduli and Poisson's ratios of

(a) (b)

Figure 4: Photographs of Grottoes 14 and 29. (a) Grotto 14. (b) Grotto 29.

Table 8: Contents of various minerals in samples of Grottoes 14 and 29

Grotto number	Weathering grade	Velocity ratio	Contents of minerals/%					
			Quartz	Feldspar[a]	Kaolinite	Calcite	Ankerite	Others
14	3	0.75	51.3	23.4	13.7	6.3	2.4	2.6
29	6	0.50	58.4	9.1	27.2	—	—	4.1

[a] Feldspar concludes K-feldspar and Na-feldspar.

K-feldspar and Na-feldspar in the horizontal direction were significantly greater than those of feldspars in the vertical direction. This is because the K-feldspar and Na-feldspar have the strongest bonds, or the Al–O bond and the Si–O bond in their silicate structures increase the intrinsic lattice resistance of dislocation. Therefore, feldspar–quartz sandstone composed of K-feldspar and Na-feldspar has an initial anisotropy in the microscopic scale.

From Table 5 it can be also seen that the mechanical anisotropies of K-feldspar and Na-feldspar are similar, agreeing with the isomorphism in the macroscopic scale. From Figure 1(b and c) it can be seen that both K-feldspar and Na-feldspar have tetrahedrons of $[Al–O_4]$ and $[Si–O_4]$ connected with each other to generate a chain connected with four tetrahedrons. The structural differences between K-feldspar and Na-feldspar are mainly due to the radii of ions. The greater radius of potassium ion results in more expansion of the tetrahedron frames of K-feldspar. On the contrary, the tetrahedron frames of Na-feldspar may collapse in this condition.

From Table 5 it can be seen that kaolinite has the lowest strength in the *Z* direction due to the existence of OH···O hydrogen bond that weakens the interlayer force in that direction. Therefore, kaolinite easily fails in the *Z* direction. When existing in the interlayer of kaolinite, the water molecules may furthermore weaken the interlayer hydrogen bond. Thus, from Table 6 it can be seen that the Young's modulus of halloysite decreases by 75.75%, compared with that of kaolinite. In the macroscopic scale, the crystal layer of halloysite will be displayed as a tubular or curled scale shape [28].

3.4.2 Microscopic mechanism of sandstone hydration

Now we provide an explanation of the sandstone hydration. As the water molecules permeate into the crystal of minerals and bring out the cations to generate

new minerals, changes in the sandstone structure may occur both in the macroscopic scale and in the microscopic scale. The average humidity in the Yungang Grottoes are usually 40%–50% and may rise to 60%–80% after rain [1]. Moreover, the Yungang Grottoes has been polluted by the coal industry [29], which will enhance the precipitation acidity. In the acidic environment, the feldspar of the Yungang Grottoes sandstone may be hydrated as follows [30]:

$$2KAlSi_3O_8(\text{K-feldspar}) + 2H^+ + 9H_2O \rightarrow Al_2Si_2O_5(OH)_4(\text{kaolinite}) + 4H_4SiO_4 + 2K^+$$

In this chemical formula, the feldspar converts into kaolinite by the actions water molecules and hydrogen ions. Therefore, the replaced metal cations will be taken away by the acid fluid.

In hydration, the mineral strengths in the sandstone of Yungang Grottoes become weak. Four main reasons account for that in a microscope scale:

(1) From Table 6 it can be seen that as the adsorbed water molecules increase from 0 to 1, huge decreases are observed in the Young's moduli of K-feldspar and Na-feldspar. The reason is that the adsorbed polarized water molecules may disturb the cations on the crystal surface and lead to structural damage when K-feldspar and Na-feldspar start to adsorb these water molecules.

(2) From Table 6 it can be seen that as the numbers of adsorbed water molecules increase, the Young's moduli of minerals greatly decrease to 73.77%, 72.80%, 42.60% and 47.46%. Tan [31] suggested that the osmotic pressure between the inside and outside crystals caused by the concentration gradient of ions in solution transfers the water molecules from low concentration zone to high concentration zone, which may apply the repulsive forces inside the crystal and then the crystal expands. These changes may damage the original structure of the mineral crystal and lead to further declination in the mechanical properties of the sandstone.

(3) From Table 4, it can be seen that the Young's modulus of kaolinite is 28.18% and 58.07%, respectively, greater than that of K-feldspar and Na-feldspar. Nevertheless, the kaolin formed in hydration [32] is subjected to combine with water molecules and therefore has a good plasticity.

(4) The varying temperature will also cause the deterioration of the mechanical properties. From Table 7 it can be understood that as the temperature rises, the volumes of minerals increase. In the macroscopic scale, this increase may lead to the expansion of the mineral particles and to furthermore generate or expand the fractures in the sandstone.

The weakening in the strength by hydration has a significant impact on the weathering of the Yungang Grottoes sandstone. In Table 8 it can be observed that during the moderately weathering stage which is less affected less hydration, the main minerals of the sandstone are quartz and feldspar and a few calcium minerals such as calcite and ankerite. As shown in Figure 4(a), at Grotto 14, discoloration was observed on the surface of sandstone with a few cracks and light loss of material and the shapes of the sandstone carving may be clearly identified. Nevertheless, as presented in Table 8, the highly weathering stage was heavily affected by hydration, wherein the feldspar has been mostly hydrated into kaolinite; the main minerals of the sandstone are quartz and kaolinite; and calcite and ankerite decomposed. As shown in Figure 4(b) at Grotto 29 where the sandstone was restored, the surface layer has been highly weathered, leading to the strip near the surface layer; the sandstone carvings were blurred and may hardly be recognized.

3.5 Discussions

As the main minerals of Yungang Grottoes sandstone, quartz, K-feldspar, Na-feldspar and kaolinite were simulated to obtain the microscopic physical and mechanical properties using their stable configurations. The microscopic physical properties agree well with the open data set. The microscopic mechanical properties indicate that the strength of feldspar in the horizontal direction exceeds that in the vertical direction due to the distribution of the ionic bonds in a cell, the structural differences of K-feldspar and Na-feldspar lie in the radii of ions and the hydrogen bond in kaolinite cell makes it prone to fail in the Z direction. These influences may contribute to the anisotropy in the macroscopic scale. Furthermore, this study considered two factors influencing the microscopic physical and mechanical properties or water molecule and temperature. As for the absorbed water molecule, the polarized water molecule may disturb the cations and gradually increase the repulsive forces to enable the cells to expand. In addition, the water molecules in the interlayer of kaolinite may disrupt the hydrogen bond. These two types of water molecules may both damage the initial structures.

Temperature rise will enable the cell to expand in such a manner that it creates and develops more cracks in the sandstone. The microscopic damages on the mineral structures caused by the water molecule may lead to great loss in the mechanical properties of the sandstone in the macroscopic scale. Furthermore, the comparison of Grotto 14 and Grotto 29 implies that the deterioration in weathering degree may severely ruin the cultural relics if the hydration occurred in the sandstone. The physical and mechanical properties of the sandstone in the macroscopic scale are mainly dominated by those in the microscopic scale. This is one of the main motivations for the multi-scale investigations. The results herein obtained from the molecular simulations may be referable for the analysis of the microscopic mechanism of sandstone hydration in Yungang Grottoes.

4 Conclusion

In this study, taking the Yungang Grottoes sandstone as an example, quartz, K-feldspar, Na-feldspar and kaolinite were selected as the main minerals to investigate the physical and mechanical properties using simulations in the microscopic scale. The influences of water and temperature on the microscopic mechanical properties were also explored. The conclusions can be drawn as follows:

(1) The unit cell and super cell models of quartz, K-feldspar, Na-feldspar and kaolinite were established and optimized. The microscopic physical and mechanical properties of those minerals were obtained by MM simulation. The simulated results agree well with those in the published data set.
(2) The anisotropy of K-feldspar and Na-feldspar shows that their Young's moduli in the Y and Z directions are three to eight times greater than those in the X direction. Kaolinite has the lowest strength and is mostly easy to fail in the Z direction.
(3) The interlayer water has a significant influence on the Young's modulus of kaolinite. As the number of adsorbed water molecules increases, the Young's moduli of K-feldspar, Na-feldspar kaolinite and halloysite decrease in various degrees.
(4) In MD simulation under one atmospheric pressure, as the temperature rises from 243.15 to 303.15 K, the volume and density of quartz, K-feldspar, Na-feldspar and kaolinite increases and decreases, respectively.

Acknowledgments: The authors appreciate the supports from the National Key R&D Program of China (Grant No. 2019YFC1520500), Shanghai Sailing Program (19YF1415500) and Shanxi Key R&D Program (Grant No. 2018-03D31080). Special thanks to Dr Zhang Xudong from Shanghai University for his helpful comments.

References

[1] Guo F, Jiang GH. Investigation into rock moisture and salinity regimes: implications of sandstone weathering in Yungang Grottoes, China. Carbonate Evaporite. 2015;30(1):1–11.
[2] Yan SJ, Chen JQ, Dou Y, Sun P. Characteristics of Yungang Grottoes sandstone and weathering simulation tests. Geoscience. 2015;29(2):442–7. (in Chinese with English abstract).
[3] Rao SM, Brinker CJ, Ross TJ. Environmental microscopy in stone conservation. Scanning. 1996;18(7):508–14.
[4] Grafchikov AA, Aranovich LY, Shmonov VM, Zakirov IV, Kaimin EP, Zakharova EV. Experimental simulation of sandstone interaction with Na-bearing alkalic solutions in a flow regime. Geochem Int. 2004;42(6):545–60.
[5] McCabe S, Smith BJ, McAlister JJ, Gomez-Heras M, McAllister D, Warke PA, et al. Changing climate, changing process: implications for salt transportation and weathering within building sandstones in the UK. Environ Earth Sci. 2013;69(4):1225–35.
[6] Barone G, Mazzoleni P, Pappalardo G, Raneri S. Microtextural and microstructural influence on the changes of physical and mechanical proprieties related to salts crystallization weathering in natural building stones. The example of Sabucina stone (Sicily). Constr Build Mater. 2015;95:355–65.
[7] Sato M, Hattanji T. A laboratory experiment on salt weathering by humidity change: salt damage induced by deliquescence and hydration. Prog Earth Planet Sci. 2018;5(84):1–10.
[8] Wang XS, Wan L, Huang JZ, Cao WB, Xu F, Dong P. Variable temperature and moisture conditions in Yungang Grottoes, China, and their impacts on ancient sculptures. Env Earth Sci. 2014;72(8):3079–88.
[9] Yang XJ, Wang JM, Zhu C, He MC. Effect of water on long-term strength of column rocks based on creep behavior in Yungang Grottoes, China. Geotech Geol Eng. 2019;37(1):173–83.
[10] Yang HM, Qiu JT, Yu L, Li PJ, Xu CB, Li WW. Spectral characteristics of chemically weathered sandstones in the Yungang Grottoes, China. Stud Conserv. 2019;64(2):63–72.
[11] Hsieh YM, Li HH, Huang TH, Jeng FS. Interpretations on how the macroscopic mechanical behavior of sandstone affected by microscopic properties – revealed by bonded-particle model. Eng Geol. 2008;99(1–2):1–10.
[12] Meng TH. Comprehensive research analysis on weathering of Yungang Grottoes [PhD thesis]. Beijing: China University of Geosciences (Beijing); 2014. (in Chinese with English abstract).
[13] Crystallography Open Database, http://www.crystallography.net/cod/index.php.

[14] Song CR, Jang WG. Cell size effects in characterizing dry quartz sand particles. Geo-congress 2008. Loui-siana, NO: America Society of Civil Engineers; 2008. p. 998–1005.
[15] Casewit CJ, Colwell KS, Rappe AK. Application of a universal force field to main group compounds. J Am Chem Soc. 114(25):10046–53.
[16] Kaplan IG. Intermolecular Interactions: Physical Picture, Computational Methods and Model Potentials. England: John Wiley & Sons; 2006. p. 149–50.
[17] Holzmann M, Bernu B. Optimized periodic 1/r Coulomb potential in two dimensions. J Comput Phys. 2004;206(1):111–21.
[18] Theodorou DN, Suter UW. Atomistic modeling of mechanical properties of polymeric glasses. Macromolecules. 1986;19(1):139–54.
[19] Chung DH, Buessem WR. The voigt reuss hill (VRH) approximation and the elastic moduli of polycrystalline ZnO, TiO_2 (rutile), and α-Al_2O_3. J Appl Phys. 1968;39(6):2777–82.
[20] Hill R. The elastic behaviour of a crystalline aggregate. Proc Phys Soc Sect A. 1952;65(5):349–54.
[21] Zhang XD, Jiang W. Lattice stabilities, mechanical and thermodynamic properties of Al_3Tm and Al_3Lu intermetallic under high pressure from first-principles calculations. Chin Phys B. 2016;25(2):026301.
[22] Hoover WG. Canonical dynamics: equilibrium phase-space distributions. Phys Rev A At Mol Opt Phys. 1985;31(3):1695–7.
[23] Berendsen HJC, Postma JPM, van Gunsteren WF, DiNola A, Haak JR. Molecular dynamics with coupling to an external bath. J Chem Phys. 1984;81:3684–90.
[24] Ichikawa Y, Kawamura K, Fujii N, Nattavut T. Molecular dynamics and multiscale homogenization analysis of seepage/diffusion problem in bentonite clay. Int J Numer Methods Eng. 2002;54(12):1717–49.
[25] Kaercher P, Militzer B, Wenk HR. Ab initio calculations of elastic constants of plagioclase feldspars. Am Miner. 2014;99(11-12):2344–52.
[26] Teppen BJ, Rasmussen K, Bertsch PM, Miller DM, Schäfer L. Molecular dynamics modeling of clay minerals. 1. Gibbsite, kaolinite, pyrophyllite, and beidellite. J Phys Chem B. 1997;101(9):1579–87.
[27] Xi DY, Liu B, Tian XY. Anisotropy and nonlinear viscoelastic behavior of saturated rocks. Chin J Geophysics. 2002;45(1):109–17. (in Chinese with English abstract).
[28] Joussein E, Petit S, Churchman J, Theng B, Righi D, Delvaux B. Halloysite clay minerals – a review. Clay Min. 2005;40(4):383–426.
[29] Salmon LG, Christoforou CS, Gerk TJ, Cass GR, Casuccio GS, Cooke GA, et al. Source contributions to airborne particle deposition at the Yungang Grottoes, China. Sci Total Environ. 1995;167(1–3):33–47.
[30] Bauluz B, Mayayo MJ, Yuste A, González López JM. Genesis of kaolinite from Albian sedimentary deposits of the Iberian range (NE Spain): analysis by XRD, SEM and TEM. Clay Min. 2008;43(3):459–75.
[31] Tan LR. Study on mechanism of expansion and shrinkage of the montmorillonite crystal. Rock Soil Mech. 1997;18(3):13–18. (in Chinese with English abstract).
[32] Lanson B, Beaufort D, Berger G, Bauer A, Cassagnabere A, Meunier A. Authigenic kaolin and illitic minerals during burial diagenesis of sandstones: a review. Clay Min. 2002;37: 1–22.